RSC Advances

PAPER

View Article Online
View Journal | View Issue

Cite this: *RSC Adv.*, 2017, **7**, 51281

Synthesis of different structured $FePO_4$ for the enhanced conversion of methyl cellulose to 5-hydroxymethylfurfural

Yong Liu,[a] Zili Li,[a] Yaohui You,[a] Xiaogang Zheng*[a] and Jing Wen *[b]

Received 19th August 2017
Accepted 30th October 2017

DOI: 10.1039/c7ra09186a

rsc.li/rsc-advances

$FePO_4$ catalysts with branch-like, flower-like, and spherical morphologies were synthesized for the conversion of methyl cellulose to 5-hydroxymethylfurfural (5-HMF) *via* a hydrothermal route. The molar ratio of Fe^{3+} and $H_2PO_4^-$ ions in the reaction system played a crucial role in the morphology of $FePO_4$. Compared with flower-like, spherical and amorphous $FePO_4$, branch-like $FePO_4$ presented a better catalytic performance in the cellulose conversion and 5-HMF yield. The branch-like $FePO_4$ retained a branch structure after recycling five times in the bi-phasic reaction process. The insolubility of low temperature and partial dissolution of elevated temperature were responsible for the excellent catalytic activity of the $FePO_4$ phase-change catalyst. The combined effect of H^+ ions and iron species generated from the hydrolysis of $FePO_4$ can be favorable for the enhanced yield of 5-HMF.

1. Introduction

Due to the growing environmental awareness of greenhouse gas and the diminishing supply of petroleum resources, the catalytic conversion of renewable biomass feedstock into fuels, chemicals, and solvents is an alternative route to relieve the reliance on fossil resources.[1,2] Many efforts focus on the development of innovative strategies for the transformation of biomass into chemicals to conquer the drawbacks including extensive, environmentally harmful, and high-cost pretreatment. Conversion of cellulosic biomass to 5-hydroxymethylfurfural (5-HMF) has triggered increasing attention.[3–5] 5-HMF, as a platform chemical, can be converted into valuable chemicals and fuels such as 2,5-furandicarboxylic acid, 2,5-dimethylfuran, and levulinic acid.[6–10]

Compared with fructose and glucose, cellulose composed of linear glucose polymer chains is an ideal feedstock for the synthesis of 5-HMF due to its low cost and abundant resources.[11,12] However, the poor solubility of cellulose and the formation of humins in aqueous media and organic solvents leads to the inferior conversion of cellulose and the low yield of 5-HMF in the catalytic system assisted with mineral acid.[13–17] Ionic liquids combined with metal salts have been confirmed to break down the inferior conversion of cellulose into 5-HMF. Ionic liquids such as [Bmim]Br, [Bmim]Br, [EMIM]Cl, and imidazolium chloride ($[C_4C_1im]Cl$, $[C_2C_1im]Cl$, and $[C_4C_1im]HSO_4$) present superior medium for the conversion of biomass feedstock due to their specific chemical and physical properties.[18–25] Nevertheless, the hybrid reaction system of ionic liquids and metal salts is not suitable for the large-scale synthesis due to the high energy consumption, high cost, and environmental contamination.

Biphasic reaction systems[26,27] and heterogeneous catalysis[28–30] have been developed to address above challenges. These strategies are more suitable and cost effective for the large-scale transformation of cellulose into 5-HMF. However, these synthesis approaches usually suffer from the serious pollution and low 5-HMF yield if the cellulose and catalysts are not pretreated in biphasic system.[31,32] This's ascribed to the insufficient contact and interaction between active sites of solid acid and insoluble cellulose in water and most organic solvents.[33,34] Therefore, the phase transfer catalyst has been developed to achieve high conversion of cellulose into 5-HMF.[35–38] The phase catalyst is characterized by the excellent activity of homogeneous acid catalyst and the effective separation and recovery of heterogeneous solid acid catalyst.[39,40] Cellulose hydrogenation reaction assisted with H_2WO_4 and Ru/C presents the maximized yield of ethylene glycerol due to the effective contact between insoluble cellulose and soluble H_2WO_4 catalyst.[29]

Iron phosphate ($FePO_4$) is a promising and inexpensive phase transfer catalyst for the efficient catalytic conversion of carbohydrates (such as glucose, fructose, and cellulose) into 5-HMF in biphasic system.[36,37] $FePO_4$ bulks are dissolved and transferred from solid state into the aqueous phase at high temperature (>140 °C), and re-precipitated to form solid bulks after cooling down to room temperature. Hence, this insolubility at room temperature and the partial dissolution at

[a]*College of Chemistry and Chemical Engineering, Neijiang Normal University, Neijiang, Sichuan 641100, China. E-mail: zhengxg123456@163.com; Fax: +86 0832 2341577; +86 0971 7762180; Tel: +86 0832 2341577; +86 0971 7762180*

[b]*Key Laboratory of Comprehensive and Highly Efficient Utilization of Salt Lake Resources, Qinghai Institute of Salt Lakes, Chinese Academy of Sciences, Xining 810008, China. E-mail: wj580420@163.com*

elevated temperatures of $FePO_4$ can surmount the drawback of recycling and separation of homogeneous catalysts. The architecture of $FePO_4$ may be crucial to the physical and chemical properties for the catalyzed synthesis of 5-HMF from cellulose during biphasic reaction process compared with $CrPO_4$ and $CrCl_3$ catalysts.[20,28,38] This is attributed to the accelerated diffusion rate of molecules and the effective exposure of active sites to reactants. For example, the ordered mesoporous structure of Nb_4W_4 exhibits high amounts of Brønsted and Lewis acid sites, leading to the excellent catalytic performance in glucose conversion into 5-HMF.[39] Due to the mesoporous structure and strong Brønsted acid sites, the mesoporous Nb_2O_5–WO_3 and Ta_2O_5–WO_3 catalysts also presented remarkable catalysis performance.[40,41] However, the new insights into the effect of $FePO_4$ microstructure on the chemical transformations of biomass feedstock remains elusive. The fundamental studies in the effect of $FePO_4$ structure on the conversion of cellulose to 5-HMF in biphasic catalytic system is also scarce.

This work focused on the controllable synthesis of $FePO_4$ for the catalytic conversion of methyl cellulose into 5-HMF. The branch-like, flower-like, and sphere $FePO_4$ were prepared in a hydrothermal system with different molar ratio of $FeCl_3$ and KH_2PO_4. The catalytic mechanism of $FePO_4$ was also proposed for the conversion of methyl cellulose to 5-HMF.

2. Experimental

2.1. Reagents

Ferric chloride ($FeCl_3$), potassium dihydrogen phosphate (KH_2PO_4), polyvinyl pyrrolidone (PVP, M_w = 58 000), absolute ethanol (C_2H_5OH), methyl cellulose (1.0×10^5 mPa s, CAS: 9004-67-5), tetrahydrofuran (THF, C_4H_8O), and sodium chloride (NaCl) were purchased from Aladdin Industrial Corporation. These chemicals were of analytical grade without any further purification.

2.2. $FePO_4$ preparation

$FePO_4$ with branch-like, flower-like, and sphere structure were prepared by a hydrothermal route with different molar ratios of $FeCl_3$ and KH_2PO_4 (1 : 3, 2 : 3, and 3 : 3). Typically, 2.0 mmol $FeCl_3$, 6.0 mmol KH_2PO_4, and 1.5 g PVP were dissolved in 60 mL ethanol solution (50 wt%) and stirred at room temperature for 3 h. Then, the above solution was transferred into a 100 mL Teflon-lined stainless autoclave and treated at 170 °C for 12 h. After cooling to room temperature, the obtained sample was centrifuged, washed with deionized water, dried at 60 °C for 10 h, and calcined at 500 °C for 3 h. Amorphous $FePO_4$ was prepared by the precipitation route.

2.3. Methyl cellulose conversion

The conversion of methyl cellulose into 5-HMF over $FePO_4$ catalysts were performed in a 200 mL stainless steel autoclave under the N_2 atmosphere of 5 bar and the given reaction temperature. Typically, 3.0 g NaCl and the given content of $FePO_4$ and methyl cellulose were added to the mixed solution of 45 mL deionized water and 135 mL THF (TMF solution of 75%), and then stirred at room temperature for 2.0 h. The above mixture was placed into a 200 mL autoclave under the given test conditions. After cooled down to room temperature, the products were centrifuged, washed, and separated into solid residue, aqueous phase, and organic phase. The liquid fraction was analyzed by the high-performance liquid chromatography. The catalytic stability of $FePO_4$ for the methyl cellulose converted into 5-HMF at 160 °C for 80 min was performed for five cycles under similar conditions. Before adding to the next reaction process, the used $FePO_4$ bulks were centrifuged, washed with water three times, dried at 60 °C for 12 h, and calcined at 500 °C for 3 h.

2.4. Characterization and analysis

XRD patterns of as-obtained $FePO_4$ were measured by a Bruker D8 Advance X-ray Powder Diffractometer. FI-IR spectra were obtained by a Shimadzu® FTIR spectrometer, IRPrestige-21 model. SEM images were observed using a Hitachi S-3400 field emission electron microscope. XPS spectra were recorded on a Thermo Fisher Scientific Escalab 250 spectrometer. Fe^{3+} species in aqueous solution was analyzed *via* the Inductively Coupled Plasma Optical Emission Spectrometer (ICP-OES) on Varian 710-ES equipped for axial viewing with a 1.12 megapixel CCD detector. The residue on the used $FePO_4$ was conducted in a TA Q5000 instrument with a He flow rate of 50 mL min^{-1}. Products were analyzed using an Agilent 1200 high-performance liquid chromatography equipped with an UV detector (280 nm) and a column (Zorbax SB-C18). 5-HMF and furfural were the main product and byproduct of methyl cellulose conversion, respectively. 5-HMF yield (Y) was defined as: Y (5-HMF) % = (moles of 5-HMF generated)/(glucose unit moles of methyl cellulose), where the mass of 5-HMF was the total content of 5-HMF in the water and organic phases.

3. Results and discussion

3.1. Characterization of $FePO_4$

The XRD patterns of $FePO_4 \cdot 2H_2O$ generated *via* a hydrothermal route and $FePO_4$ with different morphologies (including branch-like, flower-like, and sphere structure) were shown in Fig. 1. The typical peaks of $FePO_4 \cdot 2H_2O$ with different morphologies appeared at 2θ = 26.7°, 27.6°, 28.9°, 34.7°, 39.6°, 44.5°, 48.6°, 52.1°, 55.2°, 57.6°, 64.0°, and 73.3°, which were matched well with crystalline $FePO_4 \cdot 2H_2O$ phases (JCPDS no. 002-0250).[42,43] The peaks of $FePO_4$ samples at 2θ = 20.2°, 25.8°, 26.7°, 28.9°, 35.5°, 38.6°, 41.4°, 48.5°, 58.2°, and 65.7° were ascribed to the (100), (011), (012), (111), (110), (112), (200), (114), (212), and (124) planes of hexagonal $FePO_4$ samples (JCPDS no. 29-0715), respectively.[42–44] The (011) plane of $FePO_4$ at 25.8° showed stronger peak intensity compared with other peaks in XRD pattern (Fig. 1), indicating that the $FePO_4$ samples prepared *via* the hydrothermal route favored the growth along the (011) plane. The minor peak around 30.4° of fresh $FePO_4$ was ascribed to the typical peak of $Fe_4(P_2O_7)_3$ phase (JCPDS no. 24-0526).[42,45] Additional diffraction peaks of impurity were not detected in XRD patterns of $FePO_4$, meaning that the as-

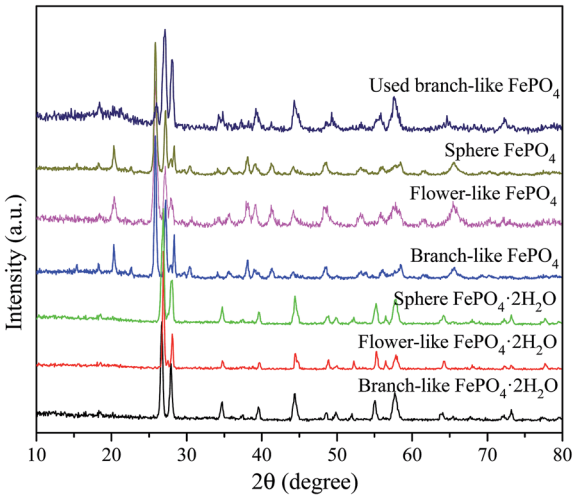

Fig. 1 XRD patterns of $FePO_4 \cdot 2H_2O$ and $FePO_4$.

prepared sample is pure $FePO_4$. The typical peaks of $FePO_4$ phases and $FePO_4 \cdot 2H_2O$ phases were detected in used branch-like $FePO_4$ bulks for the conversion of methyl cellulose into 5-HMF after five cycled times. It's suggested that the new crystalline bulks were generated *via* the dissolution and recrystallization of branch-like $FePO_4$ in the hydrothermal system.

As shown in Fig. 2, the bands around 1630 cm^{-1} as well as the bands approximately 3400 cm^{-1} of all $FePO_4$ samples were ascribed to the O–H vibration of adsorbed water molecules, while these typical bands of branch-like $FePO_4 \cdot 2H_2O$ exhibited at 1635 and 3328 cm^{-1}. Compared with amorphous $FePO_4$ bulks, the branch-like, flower-like, and sphere $FePO_4$ samples presented slight difference in FT-IR spectrum. The asymmetric stretching vibration of PO_4 group was detected at around 1090 cm^{-1}. The bands at 1020 and 940 cm^{-1} arisen from the symmetric PO_4-stretching mode associated with the Q^0 PO_4^{3-} tetrahedral.[38] The peaks at 898 cm^{-1} of amorphous and flower-like $FePO_4$ were also assigned to the symmetric stretching mode of PO_4 group. Due to the difference in morphology, the peaks below 600 cm^{-1} of all $FePO_4$ samples were related with the different Fe–O and P–O bending and stretching modes, leading to the different catalytic activity.

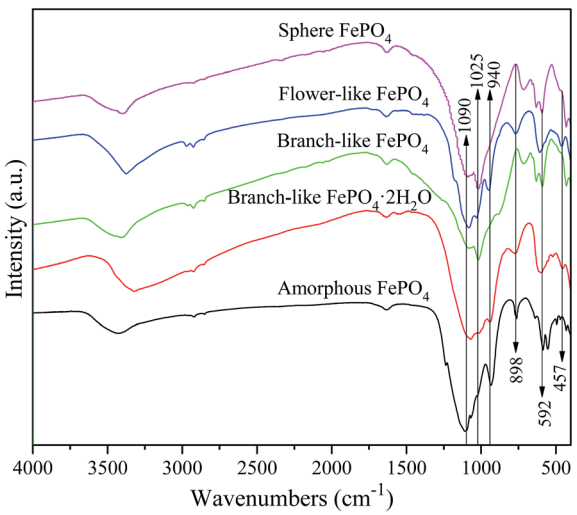

Fig. 2 FT-IR spectra of branch-like $FePO_4 \cdot 2H_2O$ and different structured $FePO_4$.

Fig. 3 presents the SEM images of $FePO_4$ with different morphologies. The branch-like, flower-like, and sphere $FePO_4$ were successfully achieved with the $FeCl_3/KH_2PO_4$ molar ratio of 1 : 3, 2 : 3, and 3 : 3, respectively. The branch-like $FePO_4$ (Fig. 3A–D) was consisted of four main branch, of which the length and the width were 10 μm and 2 μm, respectively. The flower-like $FePO_4$ with the particle diameter of around 10 μm (Fig. 3E–H) was regularly formed from small branch structure of 200 nm. Sphere $FePO_4$ (Fig. 3I–L) with a diameter of 15 μm was consisted of small nanoparticles (<50 nm). The branch-like and flower-like $FePO_4$ exhibited smooth surface structure (Fig. 3D and H), while the sphere $FePO_4$ was rough surface structure (Fig. 3L).

The formation of different structured $FePO_4$ was related with the molar ratio of Fe^{3+} and $H_2PO_4^-$ ions in hydrothermal system. Surfactant PVP serving as the structure-directing molecule also played a crucial role in the synthesis of $FePO_4$ with desired morphologies.[46–48] $FePO_4$ nanocrystallites generated from Fe^{3+} and PO_4^{3-} ions were adsorbed by PVP and then aggregated in a certain direction. Due to the reduced surface free energies of the special crystal facets, the well-matched $FePO_4$ particles with similar surface energy were assembled into oriented structure with the increase temperature.[46,49] The increasing H^+ ions released from $H_2PO_4^-$ could destroy the intrinsic crystal structure such as branch-like structure and change the surface energy of $FePO_4$ nanocrystallites. These escaping nanocrystallites went into solution of excess H^+ ions, nucleated and grew in a preferential direction with the assistance of surfactant, leading to the formation of flower-like and sphere $FePO_4$.[49] The molar ratio of Fe^{3+} and $H_2PO_4^-$ ions thus affected the morphology of $FePO_4$ in PVP-assisted hydrothermal system.

As shown in Fig. 4A–C, the used branch-like $FePO_4$ after first cycle time retained four main branch structure with less nanosheets due to the partial dissolution in reaction system at high temperature. The branch structure of $FePO_4$ was destroyed after the fifth cycle time under same conditions, and small particles randomly and gradually precipitated on the branch surface from the aqueous phase (Fig. 4D–F). It's indicated that $FePO_4$ was partially dissolved at elevated temperature and randomly precipitated again in cooling process.

The XPS spectra of different structured $FePO_4$ were exhibited in Fig. 5. The binding energies (BE) of Fe 2p and P 2p of these $FePO_4$ samples were not shifted, while the BE of O 1s were slightly shifted, as shown in Fig. 5A–C. For branch-like $FePO_4$ (Fig. 5D), the peaks at 726.1, 712.4, and 717.9 eV were assigned to the Fe 2p1/2, Fe 2p3/2, and satellite signal peaks, respectively.[43,46] It's suggested that the Fe(III) element presented in fresh $FePO_4$. The P 2p peak (Fig. 5E) was located at 133.7 eV, which was in agreement with previous work.[43] Two oxygen signals of branch-like $FePO_4$ generated from lattice oxygen and hydroxyl oxygen were observed at 531.5 and 533.0 eV in O 1s spectrum (Fig. 5F). As shown in Fig. 5C, the O 1s peaks (lattice

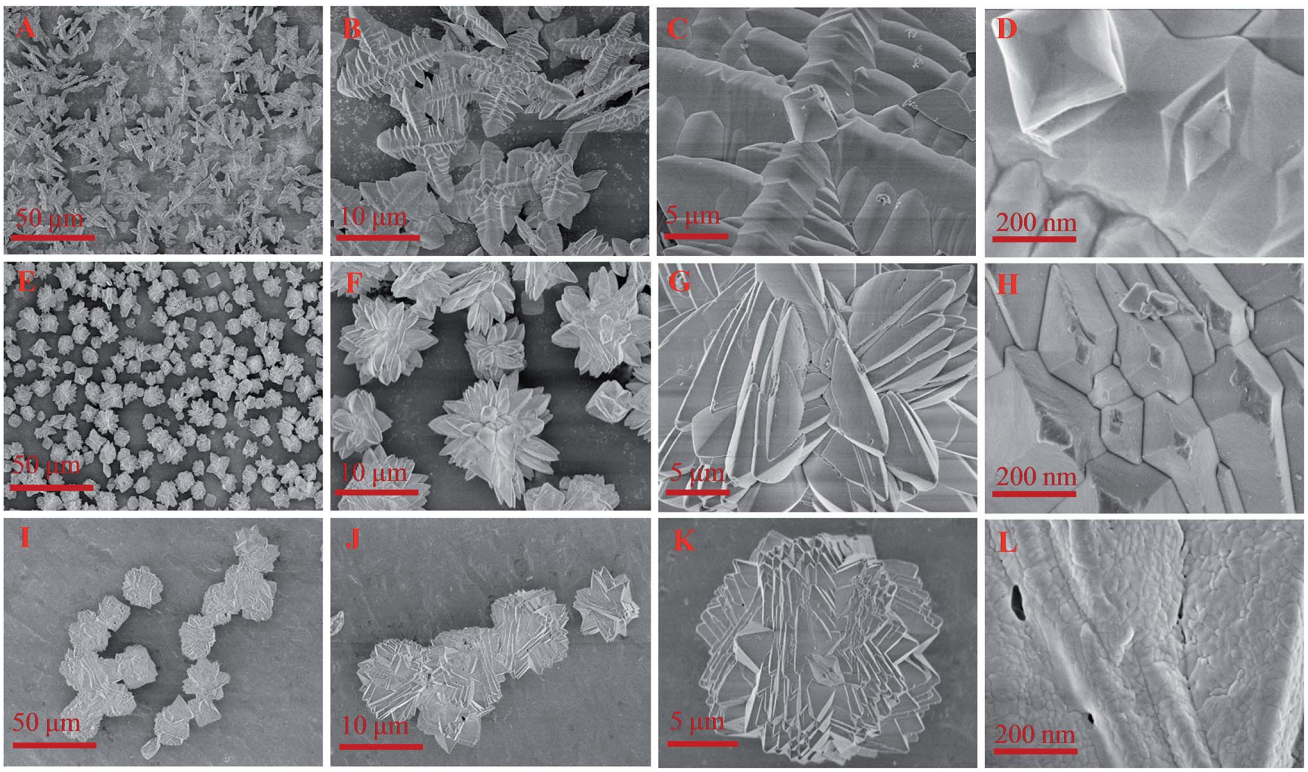

Fig. 3 SEM images of branch-like (A–D), flower-like (E–H), and sphere (I–L) $FePO_4$.

oxygen) of sphere, flower-like, and amorphous $FePO_4$ were located at 531.9, 531.7, and 531.4 eV, respectively. This slight BE variation of O 1s peaks was attributed to the difference in atomic ratio of lattice oxygen and hydroxyl oxygen of $FePO_4$ with different morphologies.

3.2. Conversion of methyl cellulose into 5-HMF

The phase-transfer catalysts such as H_2WO_4 and $FePO_4$ are effective for the cellulose converted into 5-HMF in biphasic system composed of organic solvents and water.[35,37] In the NaCl-assisted biphasic system, the cellulose contacted with soluble

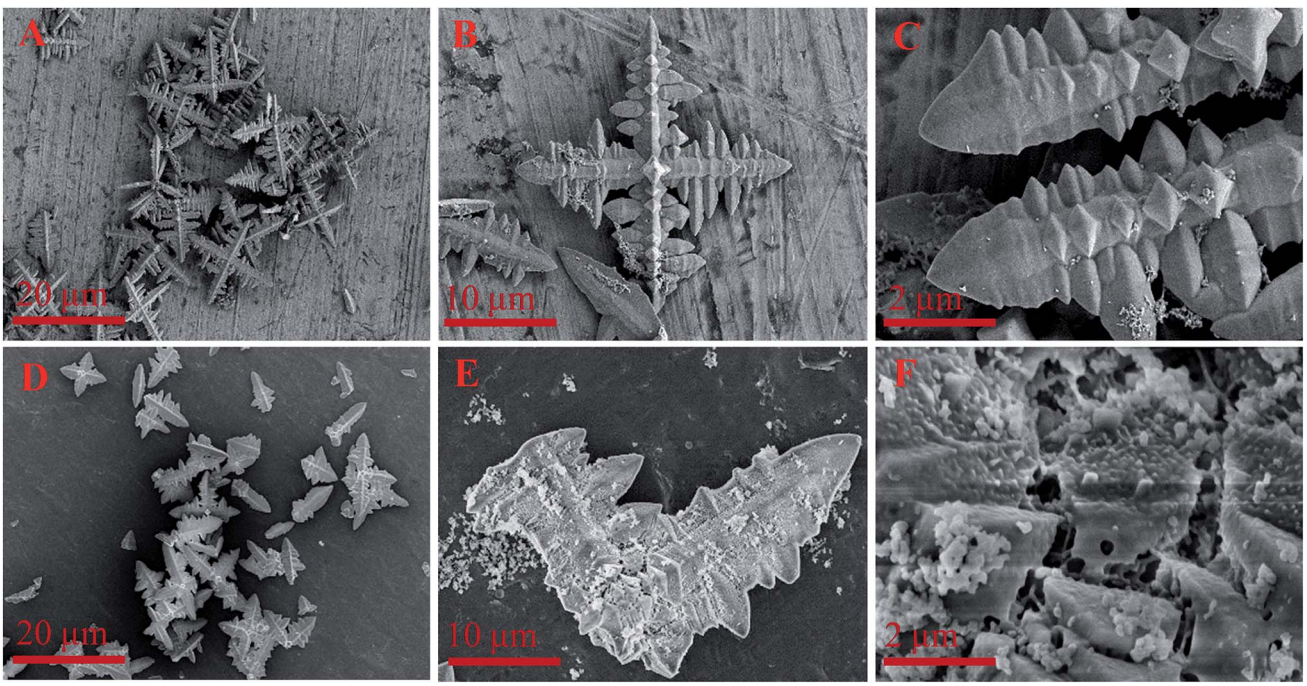

Fig. 4 SEM images of used branch-like $FePO_4$ after first (A–C) and fifth (D–F) cycled times.

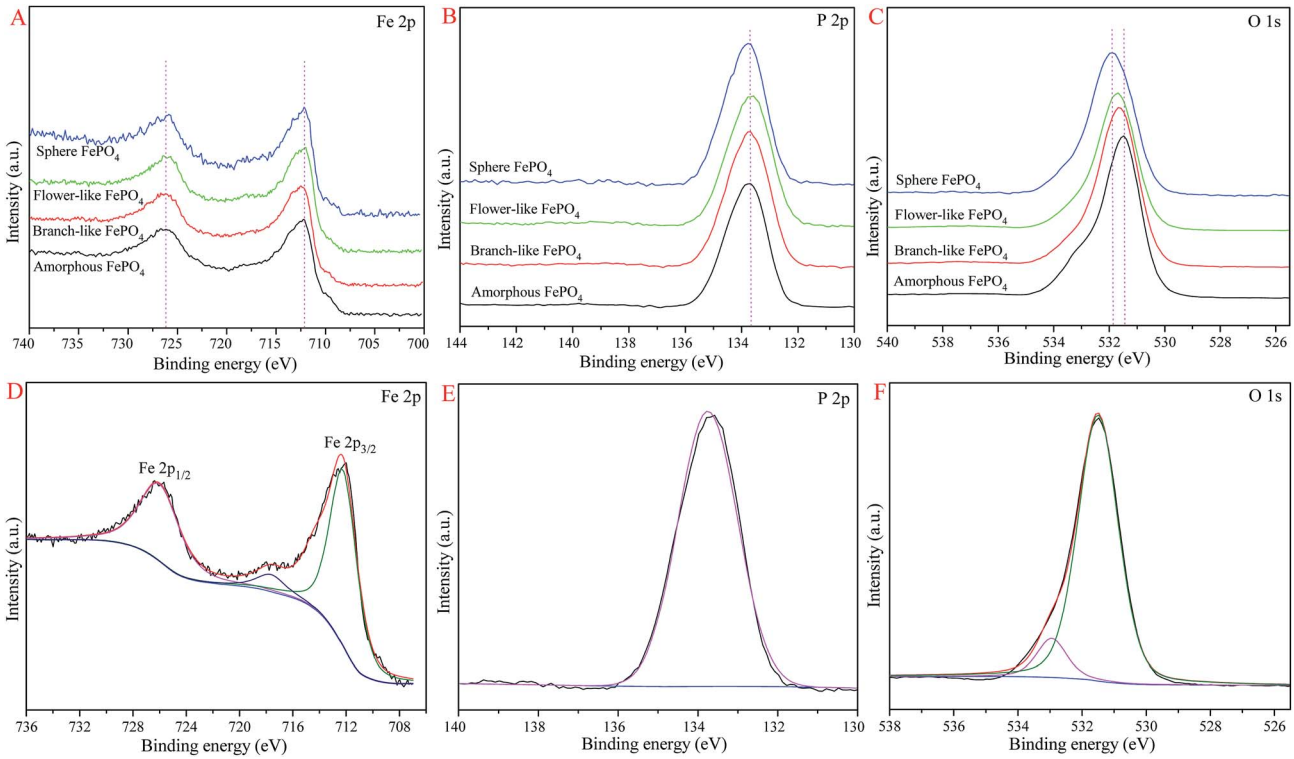

Fig. 5 XPS spectra of different structured $FePO_4$ (A–C) and branch-like $FePO_4$ (D–F).

catalyst is converted into 5-HMF in the water phase, and then the obtained 5-HMF is rapidly extracted into organic phase to avoid side reaction.[28,47,48] The optimal conversion conditions of methyl cellulose into 5-HMF were investigated in a biphasic reaction system combined with different structured $FePO_4$.

The 5-HMF yield increased with the increase of $FePO_4$ content ranged from 0.03 to 0.18 g, and slightly decreased when the $FePO_4$ dosage increased from 0.18 to 0.24 g, as shown in Fig. 6. In contrast with amorphous, sphere, and flower-like $FePO_4$, the branch-like $FePO_4$ was much more suitable for the methyl cellulose converted into 5-HMF. The highest 5-HMF yield was observed in the presence of 0.18 g branch-like $FePO_4$. It could be ascribed to the effective contact between insoluble methyl cellulose and soluble Fe^{3+} ions in the biphasic system.[36,37] The inferior 5-HMF yield for the conversion of methyl cellulose was obtained by the solid catalyst at low reaction temperature. With the increasing $FePO_4$ amount, the excess Lewis acid sites formed upon elevating temperature (160 °C) was likely to catalyze 5-HMF to undesired products such as furfural, formic acid and levulinic acid, leading to a lower 5-HMF yield.[6,20] Due to the sealed chamber and specific reaction conditions in hydrothermal system, it's difficult to detect the pH values of catalytic reaction process in this work. After cooling to room temperature, the pH values of these systems (Table 1) were slightly changed from 5.13 to 6.03 due to the poor insolubility of $FePO_4$.

The 5-HMF yield increased with the reaction time varied from 30 min to 80 min, while decreased in a reaction time range of 80–150 min, as shown in Fig. 7. Among these different structured $FePO_4$, the branch-like $FePO_4$ exhibited the best catalytic activity for the conversion of methyl cellulose. This could be related with the contact efficiency between dissoluble Fe^{3+} ions and insoluble methyl cellulose molecules. The release rate of Fe^{3+} ions in water phase was greatly affected by the morphology of $FePO_4$ at high temperature. $FePO_4$ bulks were gradually dissolved in water phase with increasing reaction time at specified temperature (such as 160 °C), leading to an

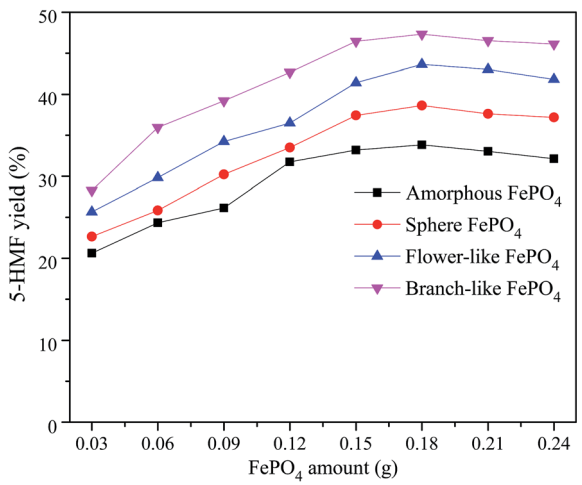

Fig. 6 Effect of $FePO_4$ content on the 5-HMF yield and pH value (methyl cellulose concentration of 2.5 g L^{-1}, reaction temperature of 160 °C, reaction time of 80 min, THF solution volume of 180 mL, and NaCl dosage of 3.0 g).

Table 1 Effect of $FePO_4$ amounts on the conversion of methyl cellulose[a]

Samples	$FePO_4$ amount (g)	Fe^{3+} amount[b] (mg)	Furfural yield/%	pH value[c]
Amorphous	0.18	1.56	3.89	5.92
Flower-like	0.18	0.95	3.64	5.37
Sphere	0.18	1.38	3.52	5.67
Branch-like	0.24	1.14	4.35	5.04
	0.21	0.97	4.27	5.13
	0.18	0.83	3.34	5.26
	0.15	0.72	3.56	5.85
	0.12	0.61	3.73	6.03

[a] Conditions: methyl cellulose concentration of 2.5 g L^{-1}, reaction temperature of 160 °C, reaction time of 80 min, THF solution volume of 180 mL, and NaCl dosage of 3.0 g. [b] Fe^{3+} amount in water phase after cooling to room temperature was detected by ICP-OES. [c] pH value of solution system after cooling to room temperature.

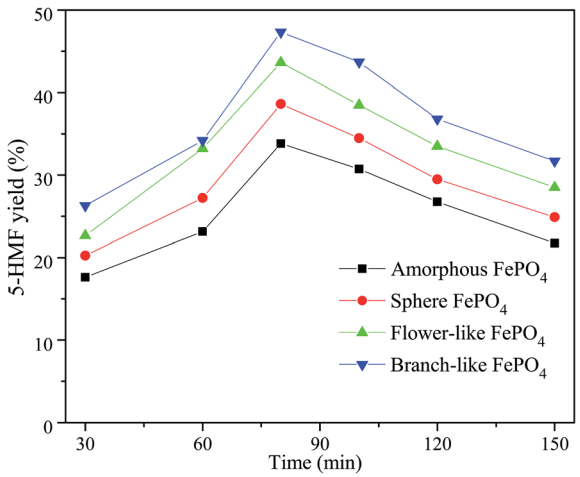

Fig. 7 Effect of reaction time on the 5-HMF yield (methyl cellulose concentration of 2.5 g L^{-1}, reaction temperature of 160 °C, $FePO_4$ content of 0.18 g, THF solution volume of 180 mL, and NaCl dosage of 3.0 g).

increasing Lewis acid sites (Fe^{3+} ions). It's reported that cellulose could be converted into furfural by Lewis acid catalysts such as Fe^{3+}, Zn^{2+}, Ca^{2+}, and Cr^{3+} ions.[26,32,51,52] These strong Lewis acid sites facilitated the formation of xylose from the retro-aldol reaction of fructose, and further converted xylose into furfural, leading to a lower 5-HMF yield.[53,54]

The effect of temperature on the 5-HMF yield over different morphological $FePO_4$ was shown in Fig. 8. 5-HMF yield increased with the reaction temperature ranged from 130 to 160 °C, while decreased with the increasing reaction temperature from 160 to 200 °C. Compared with amorphous $FePO_4$, regular structured $FePO_4$ presented excellent catalytic activity, especially the branch-like morphology. It's suggested that $FePO_4$ microstructure was responsible for the soluble rate of $FePO_4$ to release soluble Fe ions and H^+ ions. The soluble rate of branch-like $FePO_4$ consisted of nanosheets (Fig. 3A–D) was higher than that of other structures at elevated temperature,

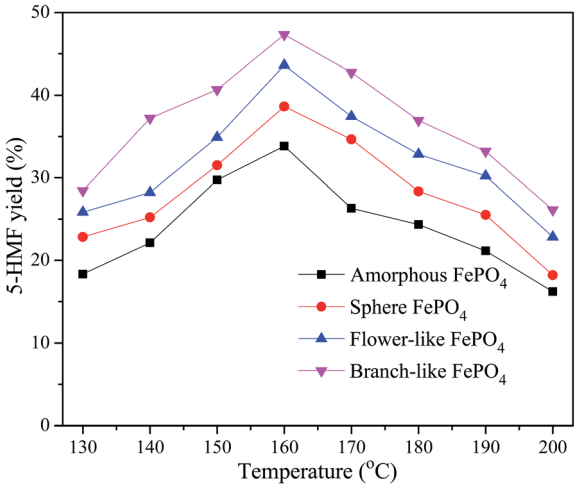

Fig. 8 Effect of reaction temperature on the 5-HMF yield (methyl cellulose concentration of 2.5 g L^{-1}, reaction time of 80 min, $FePO_4$ content of 0.18 g, THF solution volume of 180 mL, and NaCl dosage of 3.0 g).

leading to the increase of Fe^{3+} irons contacting with methyl cellulose. High level of reaction temperature favored the hydrolysis of $FePO_4$ to form Fe^{3+} irons, which were likely to catalyze 5-HMF into formic acid and levulinic acid in the water phase.

The methyl cellulose concentration as well as $FePO_4$ amounts was important for the 5-HMF yield in aqueous solvent. As shown in Fig. 9, 5-HMF yield decreased with the increasing concentration of methyl cellulose under same conditions, which was agreed with previous works.[36,37] Compared with the amorphous, flower-like, and sphere $FePO_4$, the branch-like $FePO_4$ exhibited better catalytic activity for methyl cellulose due to its higher soluble ability at 160 °C in water phase. The controllable branch-like structure could effectively restrain the

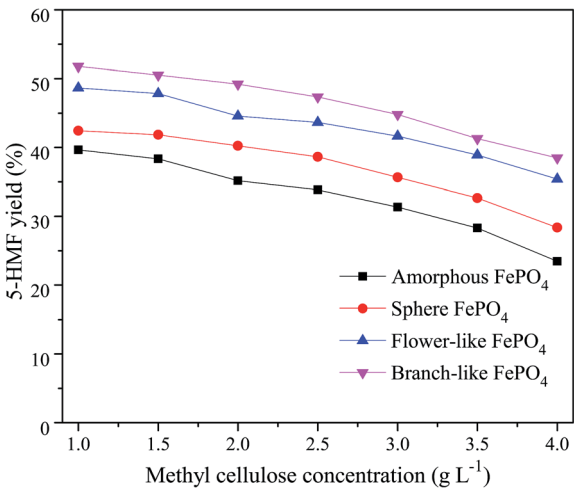

Fig. 9 Effect of methyl cellulose concentration on the 5-HMF yield (reaction temperature of 160 °C, reaction time of 80 min, $FePO_4$ content of 0.18 g, THF solution volume of 180 mL, and NaCl dosage of 3.0 g).

Table 2 Effect of methyl cellulose concentration on the residue and furfural yield[a]

Samples	Methyl cellulose concentration (g L^{-1})	Residue amount[b] (mg g_{cat}^{-1})	Furfural yield/%
Amorphous	2.5	96.5	3.89
Flower-like	2.5	75.2	3.64
Sphere	2.5	83.5	3.52
Branch-like	3.5	98.4	7.35
	3.0	65.7	5.76
	2.5	43.8	3.34
	2.0	36.9	4.58
	1.5	32.6	4.20

[a] Conditions: $FePO_4$ amount of 0.18 g, reaction temperature of 160 °C, reaction time of 80 min, THF solution volume of 180 mL, and NaCl dosage of 3.0 g. [b] Residue amount deposited on catalyst surface was detected by TGA/DTA.

dissolution rate of $FePO_4$, and further affect the H^+ ions released from the hydrolysis of Fe^{3+} ions. In addition, 5-HMF molecules were likely to react with and cross-polymerize glucose/fructose molecules to form humins during the dehydration process of methyl cellulose.[37,53,54] As listed in Table 2, higher concentration of methyl cellulose induced to the degradation of 5-HMF to humins, thereby lowering the 5-HMF yield.

The catalyst stability of $FePO_4$ for the conversion of methyl cellulose was performed five cycles at 160 °C for 80 min. The 5-HMF yield (Fig. 10A) decreased and the solid residue (Fig. 10B) increased after five cycle times. It's ascribed to the dissolved $FePO_4$ could not completely transfer into the solid phase, leading to the $FePO_4$ mass lose after cooling to room temperature.[36,37] The residue deposited on the branch-like $FePO_4$ surface was less than that of amorphous, flower-like, and sphere $FePO_4$, indicating that the branch-like $FePO_4$ retained superior catalytic activity compared with other structured $FePO_4$. As shown in Fig. 4, the solid residue was from the unreacted methyl cellulose and the humins generated from 5-HMF.[36,37] It's clearly illustrated that the $FePO_4$ was partially dissolved at the evaluated temperature, and then randomly redeposited on the $FePO_4$ surface in the temperature-fall period. The new diffraction peaks of $FePO_4 \cdot 2H_2O$ (Fig. 1) was detected in XRD pattern of used branch-like $FePO_4$, which arisen from the recrystallization of dissolved $FePO_4$.

There were three steps for the conversion of methyl cellulose into 5-HMF over $FePO_4$ catalyst in the biphasic system, as shown in Fig. 11. The methyl cellulose was depolymerized into glucose monomers by acid catalysts, then the glucose was isomerized into fructose by Lewis acid sites such as Fe^{3+} ions, and finally the fructose was dehydrated into 5-HMF over H^+ ions.[37,55] The Lewis acid sites (Fe^{3+} ions) and Brønsted acid sites (H^+ ions) generated from the hydrolysis of $FePO_4$ are thus suitable for the methyl cellulose converted into 5-HMF.[36,37] It's reported that the ion strength and temperature were crucial for the H^+ ions and soluble ions ($Fe(OH)_2^+$ and $Fe(OH)^{2+}$) released from the hydrolysis of Fe^{3+} ions.[55,56] With the elevating temperature, $FePO_4$ can partially dissolve into Fe^{3+} ions, and then hydrolyzed to soluble iron species and H^+ ions. These soluble iron species can isomerize glucose into fructose, and H^+ ions can facilitate methyl cellulose to generate glucose and catalyze fructose to 5-HMF. This indicated that the dissolved $FePO_4$ catalyst served as a "homogeneous" catalyst for the conversion of methyl cellulose. In addition, the low contact efficiency between insoluble methyl cellulose and solid $FePO_4$ active sites was also responsible for the heterogeneous catalysis reaction of methyl

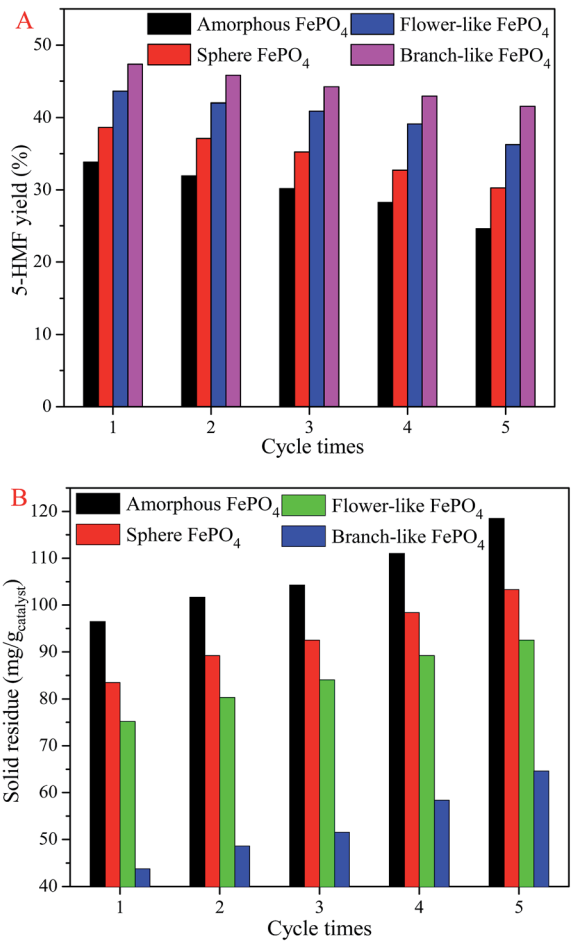

Fig. 10 Catalytic stability of $FePO_4$ for the conversion of methyl cellulose into 5-HMF (methyl cellulose concentration of 2.5 g L^{-1}, reaction temperature of 160 °C, reaction time of 80 min, $FePO_4$ content of 0.18 g, THF solution volume of 180 mL, and NaCl dosage of 3.0 g).

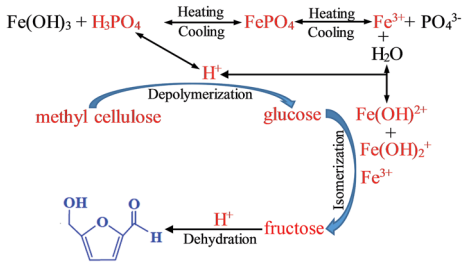

Fig. 11 Catalytic mechanism of $FePO_4$ for the conversion of methyl cellulose into 5-HMF.

cellulose into 5-HMF.[36,37,50] It's noticed that the $FePO_4$ mass loss leaded to the decreasing 5-HMF yield in the recycling process (Fig. 10). It's reasonable believed that the homogeneous catalysis of $FePO_4$ played a crucial role in the conversion of methyl cellulose.

4. Conclusion

The flower-like, branch-like, and sphere $FePO_4$ catalysts were successfully prepared *via* a hydrothermal route. Compared with amorphous, sphere, and flower-like $FePO_4$, the branch-like $FePO_4$ exhibited excellent catalytic activity and stability for the conversion of methyl cellulose into 5-HMF in the biphasic system. It's attributed to the Lewis acid sites (soluble iron species) and Brønsted acid sites (H^+ ions) generated from the dissolved $FePO_4$ at elevated temperature. The synergistic effect between iron species and H^+ ions was favorable for the excellent catalytic activity for the methyl cellulose converted into 5-HMF. This dissolved $FePO_4$ induced to the formation of $FePO_4 \cdot 2H_2O$ phase and the deterioration of branch-like structure during the phase-transfer catalytic process. The insolubility at room temperature and the dissolubility at high temperature were suitable for the potential application of $FePO_4$ in large-scale conversion of methyl cellulose into 5-HMF.

Conflicts of interest

There are no conflicts to declare.

Acknowledgements

The authors gratefully acknowledge the financial support of this work by the National Natural Science Foundation of China (Grant No.: 21506103 and 51608512), the Science and Technology Support Program of Sichuan Province (Grant No.: 2015GZ0170), the Major Training Program of the Education Department of Sichuan Province (Grant No.: 15CZ0026 and 17CZ0019), and Key Laboratory of Fruit Waste Treatment and Resource Recycling of the Sichuan Province College (Grant No.: KF17003).

References

1 R. J. van Putten, J. C. van der Waal, E. de Jong, C. B. Rasrendra, H. J. Heeres and J. G. de Vries, *Chem. Rev.*, 2013, **113**, 1499.
2 C. S. Maldonado, J. R. De la Rosaa, C. J. Lucio-Ortiz, J. S. Valente and M. J. Castaldid, *Fuel*, 2017, **198**, 134.
3 S. Xiao, B. Liu, Y. Wang, Z. Fang and Z. Zhang, *Bioresour. Technol.*, 2014, **151**, 361.
4 L. K. Ren, L. F. Zhu, T. Qi, J. Q. Tang, H. Q. Yang and C. W. Hu, *ACS Catal.*, 2017, **7**, 2199.
5 Q. Yang and T. Runge, *ACS Sustainable Chem. Eng.*, 2016, **4**, 6951.
6 V. Choudhary, S. H. Mushrif, C. Ho, A. Anderko, V. Nikolakis, N. S. Marinkovic, A. I. Frenkel, S. I. Sandler and D. G. Vlachos, *J. Am. Chem. Soc.*, 2013, **135**, 3997.
7 L. K. Ren, L. F. Zhu, T. Qi, J. Q. Tang, H. Q. Yang and C. W. Hu, *ACS Catal.*, 2017, **7**, 2199.
8 S. Jia, X. He and Z. Xu, *RSC Adv.*, 2017, **7**, 39221.
9 J. Jae, W. Zheng, R. F. Lobo and D. G. Vlachos, *ChemSusChem*, 2013, **6**, 1158.
10 H. Xin, T. Zhang, W. Li, M. Su, S. Li, Q. Shao and L. Ma, *RSC Adv.*, 2017, **7**, 41546.
11 L. Hu, G. Zhao, X. Tang, Z. Wu, J. Xu, L. Lin and S. Liu, *Bioresour. Technol.*, 2013, **148**, 501.
12 H. Tang, N. Li, F. Chen, G. Li, A. Wang, Y. Cong, X. Wang and T. Zhang, *Green Chem.*, 2017, **19**, 1855.
13 R. Weingarten, A. Rodriguez-Beuerman, F. Cao, J. S. Luterbacher, D. M. Alonso, J. A. Dumesic and G. W. Huber, *ChemCatChem*, 2014, **6**, 2229.
14 R. Weingarten, J. Cho, R. Xing, W. C. Conner Jr and G. W. Huber, *ChemSusChem*, 2012, **5**, 1280.
15 Z. Hu, Y. Peng, Y. Gao, Y. Qian, S. Ying, D. Yuan, S. Horike, N. Ogiwara, R. Babarao, Y. Wang, N. Yan and D. Zhao, *Chem. Mater.*, 2016, **28**, 2659.
16 M. I. Alam, S. De, B. Singh, B. Saha and M. M. Abu-Omar, *Appl. Catal., A*, 2014, **486**, 42.
17 S. K. R. Patil, J. Heltzel and C. R. F. Lund, *Energy Fuels*, 2012, **26**, 5281.
18 E. A. Pidko, V. Degirmenci and E. J. M. Hensen, *ChemCatChem*, 2012, **4**, 1263.
19 H. Liu, H. Wang, Y. Li, W. Yang, C. Song, H. Li, W. Zhu and W. Jiang, *RSC Adv.*, 2015, **5**, 9290.
20 S. Siankevich, Z. Fei, R. Scopelliti, P. G. Jessop, J. Zhang, N. Yan and P. J. Dyson, *ChemCatChem*, 2016, **9**, 2089.
21 H. Guo, A. Duereh, Y. Hiraga, T. M. Aida, X. Qi and R. L. Smith Jr, *Chem. Eng. J.*, 2017, **323**, 287.
22 S. Siankevich, Z. Fei, R. Scopelliti, G. Laurenczy, S. Katsyuba, N. Yan and P. J. Dyson, *ChemCatChem*, 2014, **7**, 1647.
23 M. E. Zakrzewska, E. Bogel-Lukasik and R. Bogel-Lukasik, *Chem. Rev.*, 2011, **111**, 397.
24 Q. Wang, K. Su and Z. Li, *Mol. Catal.*, 2017, **438**, 197.
25 Y. Shen, J. Sun, Y. Yi, M. Li, B. Wang, F. Xu and R. Sun, *Bioresour. Technol.*, 2014, **172**, 457.
26 B. Kassanov, J. Wang, Y. Fu and J. Chang, *RSC Adv.*, 2017, **7**, 30755.
27 X. Guo, J. Tang, B. Xiang, L. Zhu, H. Yang and C. Hu, *ChemCatChem*, 2017, **9**, 3218.
28 S. Q. Xu, X. P. Yan, Q. Bu and H. A. Xia, *RSC Adv.*, 2016, **6**, 8048.
29 Z. Tai, J. Zhang, A. Wang, J. Pang, M. Zheng and T. Zhang, *ChemSusChem*, 2013, **6**, 652.
30 A. Wang and T. Zhang, *Acc. Chem. Res.*, 2015, **46**, 1377.
31 L. Y. Y. Jiang, C. M. Bohn, G. Li, D. Han, N. S. Mosier, J. T. Miller, H. I. Kenttamaa and M. M. Abu-Omar, *Org. Chem. Front.*, 2015, **2**, 1388.
32 R. Sun, T. Wang, M. Zheng, W. Deng, J. Pang, A. Wang, X. Wang and T. Zhang, *ACS Catal.*, 2015, **5**, 874.
33 M. P. Pasternak, G. K. Rozenberg, A. P. Milner, M. Amanowicz, T. Zhou, U. Schwarz, K. Syassen, R. D. Taylor, M. Hanfland and K. Brister, *Phys. Rev. Lett.*, 1997, **79**, 4409.
34 Y. Zhang, E. A. Pidko and E. J. Hensen, *Chem.–Eur. J.*, 2011, **17**, 5281.

35 Z. W. Xi, N. Zhou, Y. Sun and K. L. Li, *Science*, 2001, **292**, 1139.
36 L. Yang, X. P. Yan, S. Q. Xu, H. Chen, H. A. Xia and S. L. Zuo, *RSC Adv.*, 2015, **5**, 19900.
37 H. Xia, S. Xu, X. Yan and S. Zuo, *Fuel Process. Technol.*, 2016, **152**, 140.
38 L. Zhang and R. K. Brow, *J. Am. Ceram. Soc.*, 2011, **94**, 3123.
39 J. Guo, S. Zhu, Y. Cen, Z. Qin, J. Wang and W. Fan, *Appl. Catal., B*, 2017, **200**, 611.
40 C. Tagusagawa, A. Takagaki, A. Iguchi, K. Takanabe, J. N. Kondo, K. Ebitani, S. Hayashi, T. Tatsumi and K. Domen, *Angew. Chem., Int. Ed.*, 2010, **49**, 1128.
41 C. Tagusagawa, A. Takagaki, A. Iguchi, K. Takanabe, J. N. Kondo, K. Ebitani, T. Tatsumi and K. Domen, *Chem. Mater.*, 2010, **22**, 3072.
42 Y. Lu, T. Zhang, Y. Liu and G. Luo, *Chem. Eng. J.*, 2012, **210**, 18.
43 X. F. Guo and W. P. Ding, *J. Fuel Chem. Technol.*, 2000, **28**, 385.
44 Y. Yin, Y. Hu, P. Wu, H. Zhang and C. Cai, *Chem. Commun.*, 2012, **48**, 2137.
45 Y. D. Yu, Y. J. Zhu and J. Wu, *Mater. Lett.*, 2017, **205**, 158.
46 S. Guo, G. Zhang and J. C. Yu, *J. Colloid Interface Sci.*, 2015, **448**, 460.
47 P. Zhao, H. Liu, H. Zheng, Q. Tang and Y. Guo, *Mater. Lett.*, 2014, **123**, 128.
48 X. Zheng, S. Huang, D. Yang, H. Zhai, Y. You, X. Fu, J. Yuan, X. Zhou, J. Wen and Y. Liu, *J. Alloys Compd.*, 2017, **705**, 131.
49 P. Yang, B. Song, R. Wu, Y. Zheng, Y. Sun and J. K. Jian, *J. Alloys Compd.*, 2009, **481**, 450.
50 C. García-Sancho, I. Fúnez-Núñez, R. Moreno-Tost, J. Santamaría-González, E. Pérez-Inestrosa, J. L. G. Fierro and P. Maireles-Torres, *Appl. Catal., B*, 2017, **206**, 617.
51 J. M. J. M. Ravasco, J. A. S. Coelho, S. P. Simeonov and C. A. M. Afonso, *RSC Adv.*, 2017, **7**, 7555.
52 H. Han, H. Zhao, Y. Liu, Z. Li, J. Song, W. Chu and Z. Sun, *RSC Adv.*, 2017, **7**, 3790.
53 Q. Liu, F. Yang, H. Yin and Y. Du, *RSC Adv.*, 2016, **6**, 49760.
54 G. Raveendra, M. Surenda and P. S. Sai Prasad, *New J. Chem.*, 2017, **41**, 8520.
55 G. Li, E. A. Pidko and E. J. M. Hensen, *Catal. Sci. Technol.*, 2014, **4**, 2241.
56 R. M. Milburn, *J. Am. Chem. Soc.*, 1957, **79**, 537.